Oxide thermoelectrics: The challenges, progress, and outlook

Jian He[a] and Yufei Liu
Department of Physics and Astronomy, Clemson University, Clemson, South Carolina, 29634-0978
Ryoji Funahashi
Nanotechnology Research Institute, National Institute of Advanced Industrial Science and Technology, Ikeda, Osaka 563-8577, Japan; and CREST, Japan Science and Technology Agency, Sanbancho, Chiyoda-ku, Tokyo 102-0075, Japan

(Received 17 January 2011; accepted 28 March 2011)

Most state-of-the-art thermoelectric (TE) materials contain heavy elements Bi, Pb, Sb, or Te and exhibit maximum figure of merit, ZT~1–2. On the other hand, oxides were believed to make poor TEs because of the low carrier mobility and high lattice thermal conductivity. That is why the discoveries of good p-type TE properties in layered cobaltites Na_xCoO_2, $Ca_4Co_3O_9$, and $Bi_2Sr_2Co_2O_9$, and promising n-type TE properties in $CaMnO_3$- and $SrTiO_3$-based perovskites and doped ZnO, broke new ground in thermoelectrics study. The past two decades have witnessed more than an order of magnitude enhancement in ZT of oxides. In this article, we briefly review the challenges, progress, and outlook of oxide TE materials in their different forms (bulk, epitaxial film, superlattice, and nanocomposites), with a greater focus on the nanostructuring approach and the late development of the oxide-based TE module.

I. INTRODUCTION

While electricity remains the most convenient form of energy in the foreseeable future, heat has been an abundant but low quality source of energy as more than half of all the energy generated by mankind is lost as waste heat. The simplest technology applicable for direct heat–electricity conversion is thermoelectricity.[1] Heat emanating from various sources (e.g., solar, geothermal, and exhaust from automobiles or other industrial processes) can be directly converted into clean electricity by a thermoelectric (TE) device, which is an all-solid assembly without moving parts or greenhouse gas emissions, compact, responsive, and feasible for miniaturization. The TE device can also work reversely as a heat pump for refrigeration (heat management).

The conversion efficiency of a TE device is determined by the Carnot efficiency and the figure of merit, ZT, of the TE material.[2] Assuming a negligible contact resistance and optimized load condition, the maximum conversion efficiency of TE power generation, η, is expressed as

$$\eta = \left(\frac{T_{hot} - T_{cold}}{T_{hot}}\right)\left[\frac{\sqrt{1+ZT_m}-1}{\sqrt{1+ZT_m}+\left(\frac{T_{cold}}{T_{hot}}\right)}\right] \quad , \qquad (1)$$

where the Carnot efficiency is given as the ratio of the temperature difference between the hot-end temperature and the cold-end temperature ($T_{hot} - T_{cold}$), to T_{hot}, and T_m is the mean temperature. ZT is the material parameter of prime importance in thermoelectrics research:

$$ZT = \frac{\alpha^2 T}{\rho\kappa} = \frac{PF}{\kappa} = \frac{\alpha^2 T}{\rho(\kappa_l + \kappa_e)} \quad , \qquad (2)$$

where α is the thermopower (or Seebeck coefficient), ρ the electrical resistivity, κ the thermal conductivity (κ_l the lattice thermal conductivity and κ_e the carrier thermal conductivity), PF the power factor, and T the temperature in Kelvin. Ideally, a TE material simultaneously possesses low ρ and low κ, i.e., a "phonon glass electron crystal" (PGEC) as coined by Slack,[3] along with a large $|\alpha|$. Although there is no theoretical upper limit for ZT values, most state-of-the-art TE materials have a maximum ZT ~1–2 in their respective temperature range of operation because of the interdependence of ρ, α, and κ. In the thermoelectrics community, $ZT = 1$ is regarded as a performance benchmark for viable TE materials.

Modern thermoelectrics research dates back to Ioffe's observation in the 1950s that heavily doped semiconductors made the best TEs.[4] The theory of semiconductor physics helps establish the basic principles of thermoelectricity and also imposes several guidelines on the bulk materials suitable for TEs. The first guideline states that the degenerate semiconductors or semimetals with carrier concentrations $n \sim 10^{18}$–10^{20} cm^{-3} make good TEs because such n values maximize the PF. The second guideline states that the semiconductors with band gap $\Delta \sim 10\ k_B T_o$ make good TEs,[5] where k_B is the Boltzmann constant and T_o the operating temperature. Such a band gap size ensures a reasonable value for the carrier

[a]Address all correspondence to this author.
e-mail: jianhe@clemson.edu
DOI: 10.1557/jmr.2011.108

 © Materials Research Society 2011

https://doi.org/10.1557/jmr.2011.108 Published online by Cambridge University Press

mobility, μ, and minimizes the detrimental contribution from the minority carrier to α (i.e., the bipolar effect). Goldsmid[6] pointed out that Z is determined by $(m^*)^{1.5}\mu$, where m^* is the effective mass of carrier. Enhancing m^* without deteriorating μ leads to the third guideline: it is thermoelectrically favorable for materials to adopt a high-symmetry crystal structure (to have high band-degeneracy) and have small electronegativity difference among the constituent elements (to minimize the scattering of charge carriers by optical phonons). The fourth guideline concerns κ_l: low κ_l is often found in materials made up of heavy elements and/or with many atoms per unit cell. Most of the current state-of-the-art TE materials are in-line with these guidelines, they are degenerate semiconductor or semimetal bulk materials with high-symmetry crystal structure and contain one or more of the heavy elements Bi, Pb, Te, or Sb.

In view of these guidelines, however, oxides are believed to make poor TEs. First, the large electronegativity difference among the constituent elements leads to more ionic bonding, strong tendency for carrier localization, and strong scattering of carriers by optical phonons, the resulting μ may be orders of magnitude lower than that of the heavy element-based TE materials. Even for high mobility oxide semiconductors, $|\alpha|$ is often found to be small because of the cancellation between the electron and hole band contributions. Moreover, the large bonding energy and the small mass of oxygen lead to a high velocity of sound and, therefore, high κ_l. This is why the good TE properties found in Na_xCoO_2 are peculiar and enlightening in pursuing novel mechanisms of thermoelectricity.[7–9] Theoretical studies have suggested that the high α may be related to electron correlation[10] and high carrier (spin and orbital) degeneracy,[11,12] whereas Singh et al. argued that the high α can be explained by standard band theory on the basis of the splitting of t_{2g} manifold.[13]

In this article, we present an overview of the recent progress of oxide thermoelectrics research. A comparison is made among the performance of several representative TE oxides in their different forms such as bulk material (single crystal and polycrystal), epitaxial film, and nanostructured material [two-dimensional (2D) electron gas system, superlattice, and nanocomposite]. In particular, the rationale, strategies, and experimental results of the emerging nanostructuring approach are highlighted. Finally, we briefly discuss the status of the TE oxide module development. Readers further interested in oxide thermoelectrics research are referred to excellent reviews by Koumoto et al.,[14] Ohtaki,[15] and Ohta et al.[16]

II. OXIDE TEs

A. Merits of oxides

Although ZT of oxides is still low compared with the current state-of-the-art TE materials,[17–19] oxides possess several inherent merits from fundamental and application points of view. First, the high chemical and thermal stability of oxides allows for a large temperature gradient to be applied across the materials in air [Fig. 1(a)], thereby leading to a high Carnot efficiency in Eq. (1) that somewhat compensates the low ZT. Second, the large temperature gradient may induce novel nonlinear, nonlocal TE effects (e.g., the Benedicks effect[20]) that may be thermoelectrically favorable.[21] Third, oxides are featured by their chemical versatility and structural intricacy, which offering a great flexibility of structural and compositional tailoring. Finally, oxides are decidedly advantageous in terms of the cost of raw materials and the environmental friendliness. For any large-scale application of thermoelectricity, the cost of raw material is a major consideration after performance. For example, the increasing price of Te somewhat vitiates the enhancement of ZT in the Te-containing high-performance nanostructured TE materials.[17–19] Hence, high-performance TE materials based on abundantly available [Fig. 1(b)] and nontoxic elements with high chemical and thermal stability are crucial for any viable large-scale applications.[22] As shown in Fig. 1(a), oxides are particularly suitable for high temperature power generation in air.

B. "Hybrid crystal"

Since the discovery of the good p-type material Na_xCoO_2, a number of cobaltites with hexagonal CoO_2 sheets that are structurally similar to those in Na_xCoO_2 have been prepared and studied from the TE perspective. Promising p-type TE properties have been found in $Ca_3Co_4O_9$[23–28] and $Bi_2Sr_2Co_2O_9$.[29–32] Studies on these layered cobaltite oxides have drawn on the important concept of the "hybrid crystal"[33] in-line with the concepts of PGEC.[3] The basic idea of the "hybrid crystal" is that a complex crystal structure can be regarded as being formed by building modules with different compositions, structural symmetries, and, therefore, specific TE functions, the electrical and thermal transport can be thus somewhat decoupled and individually tuned to attain a higher ZT. As shown in Fig. 2(a), $Na_xCo_2O_4$ adopts a hexagonal-layered structure with edge-sharing 2D triangle CoO_2 sheets ("electron crystal") and highly disordered Na layers ("phonon glass") alternately stacked along c-axis. In $Ca_3Co_4O_9$ and $Bi_2Sr_2Co_2O_9$, there is a lattice misfit between the hexagonal CoO_2 sheet and the square Ca_2CoO_3 and $Bi_2Sr_2O_4$ substructures [Figs. 2(b) and 2(c)].

Another example of a "hybrid crystal" is the Ruddlesden–Popper homologous series of $Sr_{m+1}Ti_mO_{3m+1}$ in which two basic building modules, SrO and $SrTiO_3$, are alternately stacked. Promising n-type TE properties have been found in perovskite compounds with a general formula ABO_3 ($Sr_{m+1}Ti_mO_{3m+1}$ with $m = \infty$).[34–36] For example, heavily Nd-doped $SrTiO_3$ ($n \sim 10^{21}$ cm^{-3}) exhibits a large PF of 3.6×10^{-3} W·m^{-1}·K^{-2} at room

https://doi.org/10.1557/jmr.2011.108 Published online by Cambridge University Press

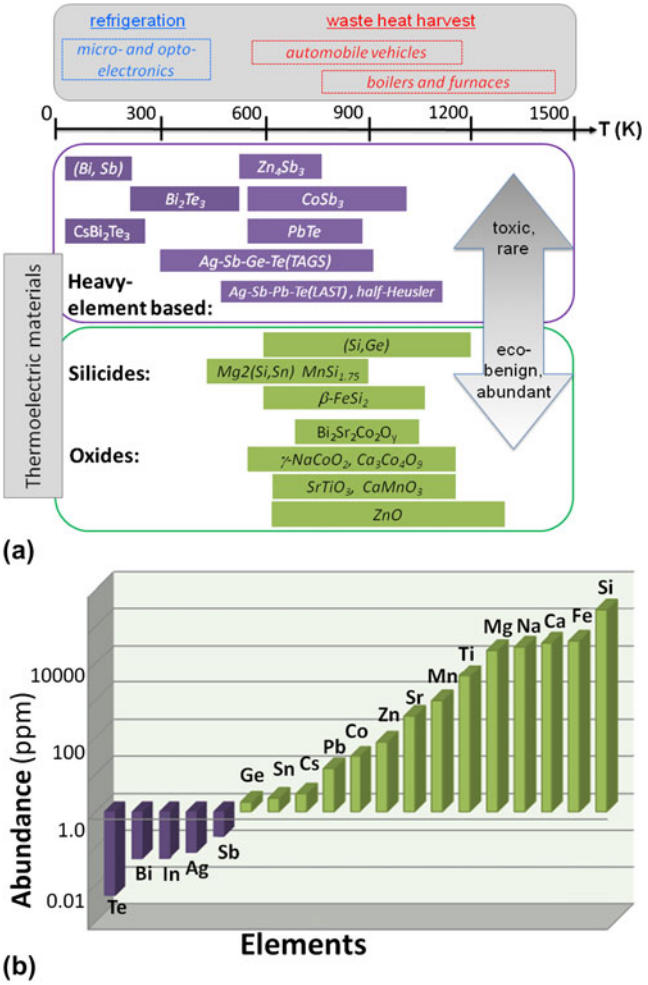


FIG. 1. (a) Schematic comparison of various thermoelectric (TE) materials for applications of waste heat harvest and refrigeration, in terms of the temperature range of operation and the abundance and environmental friendliness of constituent elements. (b) The abundance of elements used in TE materials, the elements represented by dark-colored columns are <1 ppm.

temperature because of the large density of states (DOS).[37] In particular, *ZT* of doped $CaMnO_3$ has been significantly improved since 2008.[38–41]

C. Other bulk oxides

In addition to the aforementioned layered structured cobaltites and ABO_3 perovskites, many other bulk oxides have been studied from the TE perspective, to name a few, $[(Bi,Pb)_2Ba_2O_{4\pm\omega}]_{0.5}CoO_2$,[42] $Bi_{0.78}Sr_{0.4}RhO_{3+\delta}$,[43] $La_{0.95}Sr_{0.05}CoO_3$,[44] $La_{1-x}Sr_xCrO_3$,[45] $CuRh_{1x}Mg_xO_2$,[46] doped In_2O_3,[47] Ln (rare earth)-doped SrO$(SrTiO_3)_n$,[48,49,50] Li- and Na-doped NiO,[51] Sr_xCoO_2 (x~0.35),[52] doped ZnO,[53–56] and $In_2O_3(ZnO)_m$ (m = integer).[57] Despite a wide variety of structures and compositions, these materials can be roughly grouped depending on their μ values. In contrast to In_2O_3 and ZnO with high μ values, the electrical conduction in doped $La(Co,Cr)O_3$ is due to small polaron hopping,[58] featured by μ values much lower than the band conduction and a thermal activation type behavior of ρ. Interestingly, instead of a nearly temperature-independent α as expected from a small polaron system, $La(Co,Cr)O_3$ exhibits a linear temperature dependence in α, reminiscent of the heterosite hopping in boron carbides.[59] In $La(Co,Cr)O_3$ the large difference in the spin and orbital configurations of different valence states of Co/Cr cations give rise to a large carrier degeneracy and, therefore, high α.[12]

D. Epitaxial films

The intrinsic TE properties of oxides are often difficult to determine because most of the as-synthesized oxides are in the form of small single crystals or polycrystalline ceramics. The growth of single crystals is time-consuming and expensive, whereas polycrystals usually have poorly characterized texture, grain boundaries, pores, and crystal chemistry (e.g., oxygen off-stoichiometry). Therefore, high-quality epitaxial films of several TE oxides, such as Na_xCoO_2,[60] $Ca_3Co_4O_9$,[61,62] $SrTiO_3$:Nb,[63] TiO_2:Nb,[64] and $SrO(SrTiO_3)_n$:Nb (n = 1, 2),[65] have been fabricated. In particular, a reactive solid phase epitaxy technique[66] has been developed to grow epitaxial films of p-type layered oxides containing high volatile elements. The high-quality epitaxial film is thermoelectrically favorable in that the thin film largely possesses the intrinsic electrical properties of the bulk single crystal and a lower κ because of strong phonon scatterings at boundaries. Transport properties measurements performed on these thin film samples suggest that some of the previously reported *ZT* values are questionable.[16]

It is also found that Na_xCoO_2 decomposes into insulating $Co(OH)_2$ in a high humidity environment because the Na^+ ions easily dissolve in H_2O, whereas $Ca_3Co_4O_9$ exhibits good p-type TE properties and good thermal stability at 1000 K in air. The *ZT* of epitaxial film $Ca_3Co_4O_9$ reaches ~0.3 at 1000 K,[16] which is lower than that of p-type Si–Ge (ZT~0.8).[67] The chances of further improving the *ZT* of $Ca_3Co_4O_9$ may lie in enhancing |α| via optimizing the misfit ratio.[68]

E. Two-dimensional electron gas systems and superlattices

As for the n-type films, the *ZT* of epitaxial film $SrTi_{0.8}Nb_{0.2}O_3$ reaches ~0.3 at 1000 K.[16] However, further improving the *ZT* of ABO_3 perovskites via a traditional doping approach has proved to be difficult.[69–71] Hence, a novel technical route, i.e., 2D electron gas (2DEG), has been adopted to improve *ZT* via enhancing α. In general, |α| is a measure of the energy dependence of the DOS at the Fermi level (E_F). The DOS (E_F) of transition metal oxides (TMOs) is predominated by heavy *d*-electrons, therefore, the conduction electrons are

https://doi.org/10.1557/jmr.2011.108 Published online by Cambridge University Press

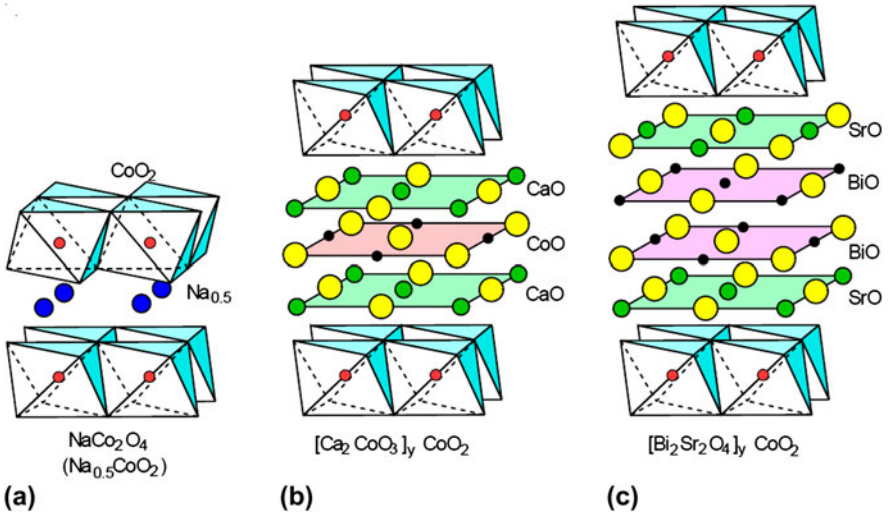


FIG. 2. Schematic crystal structures of the layered cobaltites (a) Na_xCoO_2, (b) $Ca_3Co_4O_9$, and (c) BiSrCoO. (From Ref. 33. Copyright Materials Research Society, reproduced with permission.)

expected to be localized more strongly in TMOs than in heavy element-based TE materials. In addition, quantum size effects (quantum confinement) are expected to further enhance the DOS(E_F) in a 2DEG system. Ohta et al. have fabricated a superlattice system composed of insulating $SrTiO_3$ (undoped, carrier concentration: $n < 10^{15}$ cm^{-3}) and highly conductive Nb-doped $SrTiO_3$ ($SrTi_{0.8}Nb_{0.2}O_3$, $n = 2.4 \times 10^{21}$ cm^{-3}) on the (001)-face of $LaAlO_3$ single crystal substrates by pulse laser deposition (PLD).[72,73,74] The room temperature α value is enhanced by a factor of about 5 (from -198 μV/K for bulk $SrTiO_3$ to ~ -1000 μV/K for the 2DEG system) without deteriorating σ. Assuming the κ value of the bulk single crystal, the room temperature ZT is ~2.4 for the 2DEG system, corresponding to a $ZT \sim 0.24$ for a complete device containing 2DEG as the active region. Figure 3[16] shows the Cs-corrected high-angle annular dark-field scanning transmission electron microscope image of an as-prepared superlattice system. The results of Ti-$L_{2,3}$ edge electron energy loss spectroscopy show that the Ti column in one unit cell thickness of $SrTi_{0.8}Nb_{0.2}O_3$ had a higher intensity than that of the $SrTiO_3$ barrier layer, confirming that the doped Nb^{5+} ions are exclusively confined in the $SrTi_{0.8}Nb_{0.2}O_3$ layer.

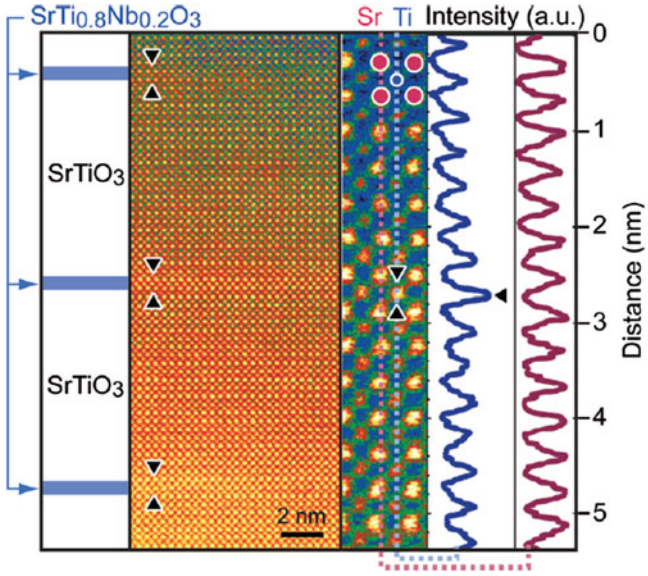


FIG. 3. High-angle annular dark-field scanning transmission electron microscope image and Ti-$L_{2,3}$ edge electron energy loss spectroscopy profile. (From Ref. 16. Copyright American Chemical Society, reproduced with permission.)

Another important 2DEG system has been fabricated at the heterointerface between oxygen-deficient $TiO_{2-\delta}$ and $SrTiO_3$. The $TiO_{2-\delta}$ film possibly extracts O^{2-} from the $SrTiO_3$ substrate, introducing conduction electrons confined at the heterointerface between TiO_2 and $SrTiO_3$. Figure 4[16] shows the depth profile for the $TiO_2/SrTiO_3$ heterointerface. The full width at half maximum of the carrier concentration peak at the heterointerface is ~0.3 nm, which is close to the lattice parameter of $SrTiO_3$ ($a = 0.3905$ nm). Hence, a high concentration of conduction electrons is localized within a unit cell thickness of $SrTiO_3$ at the heterointerface.

Both $SrTiO_3$ and TiO_2 have the TiO_6 octahedra as the basic structural module. The shape of TiO_6 octahedra in $SrTiO_3$ is regular, and the Ti 3d-t_{2g} orbitals of $3d_{xy}$, $3d_{yz}$, and $3d_{zx}$ are degenerate; the shape of TiO_6 octahedra in TiO_2 is irregular, and the $3d_{xy}$ orbital has lower energy level compared with $3d_{yz}$ and $3d_{zx}$ because of the crystal field splitting.[75] The comparison of carrier generation, transport properties, such as n, m^*, and carrier relaxation time between $SrTiO_3$ and TiO_2 is thus instructive for future selection and design of titanate-based TE oxides. Kurita et al.[64] have proposed that the titanates with a high-symmetry structure would exhibit better TE performance than the low symmetry one, which is consistent with the third guideline discussed in the Introduction.

https://doi.org/10.1557/jmr.2011.108 Published online by Cambridge University Press

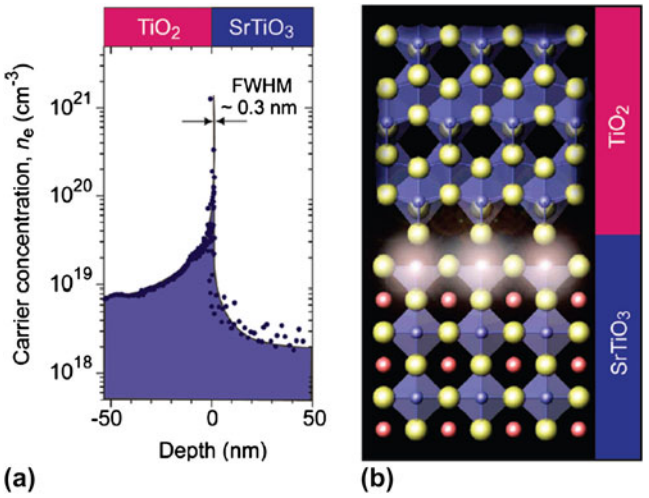


FIG. 4. (a) Depth profile across the heterointerface between a TiO_2 epitaxial layer and the $SrTiO_3$ substrate. (b) Schematic drawing of the heterointerface crystal structure. (From Ref. 16. Copyright American Chemical Society, reproduced with permission.)

To reduce the production cost and to scale up the size of 2DEG systems, Ohta et al.[76] have fabricated an amorphous oxide semiconductor superlattice comprised of α-In–Zn–O (quantum well) and α-In–Ga–Zn–O (barrier) layers on a silica glass substrate by PLD at room temperature (without substrate heating). When the thickness of the α-In–Zn–O layer is less than ~5 nm, the quantum size effects drastically enhance the room temperature $|\alpha|$ value by a factor of about 4 (from −19 μV/K to ~−73 μV/K) without deteriorating σ.

III. NANOSTRUCTURING APPROACH IN OXIDES

The above 2DEG approach is in-line with the paradigm of "nanostructured thermoelectrics" that is initiated and established in nonoxide TE materials.[17–19] This new paradigm dates back to the theoretical prediction by Hicks and Dresselhaus[77] that quantum size effects could dramatically enhance the electrical performance and the *ZT* of a low dimensional system[78] compared to its bulk counterpart. Their prediction was partly verified by the ~2.5 times enhancement of $|\alpha|$ in the PbTe (1.5 nm)/$Pb_{0.927}Eu_{0.073}Te$ (45 nm) multiple quantum well system[79] and the 2DEG and superlattice systems discussed above in section 2E.

A. Rationale for nanostructuring approach

The rationale for this nanostructuring approach is based on the impact of quantum and classical size effects on the behaviors of electrons and phonons.[80,81] While classical size effects limit the mean free paths of electrons and phonons, quantum size effects (quantum confinement) may introduce some thermoelectrically favorable change in the electronic band structure and phonon dispersion relations. Combined classical and quantum size effects can make the TE properties of a nanostructured material[82] so different from its bulk counterpart that it is eligible to be treated as a new material. The nearly two orders of magnitude improvement of *ZT* in Si nanowires[83,84] and a factor of ~3.5 improvement of *ZT* in bulk nanostructured Si are good examples. In particular, the phonon drag effect is invoked to explain the simultaneously enhanced α and reduced κ in Si nanowires as certain phonon modes drag charge carriers while carrying a minimal amount of heat,[84] it is well known, however, that the phonon drag effect has small effect on the *ZT* of bulk materials.

Note that there is an important difference between the charge transport and the heat transport in TE materials: the charge carriers are nearly monoenergetic (within a few k_BT near E_F), whereas the heat-carrying phonons are broad in energy (frequency) and momentum (wave length). As such, the charge-carrying electrons and heat-carrying phonons may be subject to a different degree of size effects, which in turn provides for an extra pathway to control the charge and heat flows. While the mean free paths and wavelengths of electrons and phonons are typically on the nanometer scale, the nanostructuring approach is evidently the option.

B. Nanocomposites: A new paradigm

To date the main gains in enhancing *ZT* in nanostructured TE materials are from the significant reduction of κ_l.[17–19] Theoretical studies show that the thermal boundary resistance and a high density of interfaces, rather than the atomically perfect interfaces or the periodicity of nanostructures, are the key ingredients for such significant reduction of κ_l.[85,86] It immediately prompts the idea of using bulk nanostructured materials (i.e., nanocomposites) as a potential cost-effective and scalable alternative to the expensive 2DEG and superlattice systems. Important advantages of nanocomposites include being made using a bulk synthesis procedure and in a form compatible with existing commercial TE devices, possessing better mechanical properties, and being more isotropic.

To date, the maximum *ZT* values achieved in p-type and n-type oxide bulk TE materials are ~1.0–1.2 and 0.6–0.7, respectively. Furthermore, the *ZT* of a single crystal is higher than that of polycrystal, and this discrepancy in *ZT* is notably larger for p-type materials than n-type materials. This observation highlights the importance of grain boundaries and intergranular connections for the TE properties of polycrystals (including nanocomposites).

The interfacial boundary scattering plays a central role in enhancing the *ZT* of a *nonoxide* nanocomposite.[87] The effective medium theory made it clear that the *ZT* of a composite can not exceed the best performing constituent if there is no contribution from the interfaces.[88] Ideally a multifold preferential scattering at interfacial boundaries should be implemented to scatter phonons more effectively than electrons as for a "PGEC" and to scatter those carriers with low mean energy more

https://doi.org/10.1557/jmr.2011.108 Published online by Cambridge University Press

effectively than those with higher mean energy for a larger |α| and *PF* in the context of the electron filtering mechanism.[89,90] Such multifold preferential scattering mechanisms can be implemented via controlling the physical parameters of the barrier at interfacial boundaries.[87]

C. Nanocomposite oxides

Note that n-type oxide bulk materials such as $SrTiO_3$ and $CaMnO_3$ have fairly high *PF* values and their low *ZT* values are due primarily to high κ_l. For example, κ_l accounts for ~80% of κ in $SrTiO_3$. For an all-oxide TE device, higher *ZT* of n-type materials are required and may be achieved primarily by reducing κ_l via the nanostructuring approach. This is the main theme of this section.

1. Nanostructuring and reducing κ_l

In several nanostructured nonoxide materials, κ_l is found to be lower than the so-called "alloy limit" of bulk thermal conductivity.[91–94] Phonons in a material have a temperature-dependent wide spectrum of wavelengths and mean free paths, all of which contribute to κ_l. Hence, it is commonly believed that a multiscale structural complexity,[95] from the atomic scale alloying and strain fields to the interfacial boundary scattering particular to nanoscale constituents, is required to effectively scatter phonons of a wide range of energies and wavelengths and over a wide temperature range. At present, a main challenge is the lack of quantitative understanding of the contribution from each scattering mechanism and the interplay between these mechanisms. As a result, the present effort is largely trial and error, modeling based on molecular dynamics and nonequilibrium Green's functions should be conducted in the future.

A recent study of the dependence of grain size and κ_l in undoped $SrTiO_3$[14] shows that κ_l decreases nearly linearly with decreasing grain size below 100 nm, and assuming this linearity holds, κ_l will reach the alloy limit with a grain size of few nanometer.[96] The grain boundaries scatter phonons at lower temperatures, and the Umklapp phonon–phonon scattering dominates at elevated temperatures. In another study, $(Ca,Yb)MnO_3$ nanoparticles with an average size of ~50 nm have been prepared using a gas-phase reaction (GPR, or flash creation method) technique[97] and then sintered at 1323 K into bulk sample of about 70% theoretical density. In the sintered sample, the average grain size is 620 nm. The $(Ca,Yb)MnO_3$ GPR-bulk sample exhibits a variable range hopping resistivity behavior, and the detrimental bipolar effect is shifted to higher temperatures compared with the bulk sample prepared by a solid state reaction.[14]

2. Nanocomposite TE oxides

An often used nanocomposite synthesis method is to incorporate a small amount of nanosized secondary phase into a bulk matrix with proved TE performance. For example, the formation of Yb_2O_3 nanoprecipitates,[98] CeO_2 nanoparticle,[99] and the addition of ZrO_2[100] into a $CoSb_3$-based bulk matrix has led to improved TE properties. The addition of Ge in In_2O_3 has led to electron doping via the Ge substitution on the In site along with the formation of $In_2Ge_2O_7$ precipitates and a reported ZT~0.45 at 1273 K.[101]

ZnO-based materials are an important class of TE oxides featured by high μ values on the order of 10–100 cm^2/Vs[54] (one of the highest reported in oxides) and high *PF*s on the order of 10^{-3} W/mK^2 (comparable to that of SiGe materials). The main challenge is to reduce κ_l without deteriorating the *PF*. Making a solid solution with MgO and NiO has proved to be unsuccessful. Because of very low dopant solubility on Zn site, addition of Al in ZnO more than 2 mol% resulted in the formation of fine precipitates of $ZnAl_2O_4$.[54,55] Ohtaki et al. recently reported a co-doping of Al and Ga in ZnO and a ZT~0.65 at 1273 K in a nanocomposite with a nominal composition of $Zn_{0.96}Al_{0.02}Ga_{0.02}O$.[56]

Koumoto's group recently reported the incorporation of nanosized yttria-stabilized zirconia,[102] mesoporous silica,[103] and potassium titanate[104] in Nb-doped $SrTiO_3$ bulk matrix and the impact on the TE properties. The results show that these additions (up to a few wt%) enhance the phonon scattering at grain boundaries, increase the electrical conductivity via promoting the packing density, thus leading to a substantial enhancement of *ZT*. On the other hand, the thermal and chemical stabilities of nanosized oxide additions in the bulk matrix deserve more investigations. For example, $Sr_2Ti_2SiO_8$ phase has a tendency to form in the Nb-doped $SrTiO_3$-mesoporous silica composite, though it helps scatter phonons more effectively.[103]

Nanocomposites can be also prepared using an in situ or self-assembly method,[105] such as spinodal decomposition and matrix encapsulation ("arrested precipitation") in nonoxide TE materials. Compared to the ex situ method, the in situ method usually leads to more coherent or semicoherent interfacial boundaries that promote μ. Along this line, heat treatment-induced phase separation has been used to prepare $Zn(Mn,Ga)O_4$ nanocomposites.[106,107] The nanocomposite is comprised of a tetragonal $ZnMn_{1.7}Ga_{0.3}O_4$ phase and a cubic $ZnMn_{0.5}Ga_{1.5}O_4$ phase. As shown in Fig. 5, they are in the form of nanorods and alternately stacked in such a way that the cross-sectional and side views show checkerboard and herringbone patterns, respectively. The average size of each nanorod is ~4 × 4 × 70 nm^3 and the average size of a grain is ~3 μm. For comparison, a microcomposite composed of $ZnMn_{1.7}Ga_{0.3}O_4$ and $ZnMn_{0.5}Ga_{1.5}O_4$ coarse grains has been prepared with an average grain size ~3.7 μm and without intragrain nanostructures. The κ_l value of the nanocomposite is not only significantly lower than that of the microcomposite but also lower than

https://doi.org/10.1557/jmr.2011.108 Published online by Cambridge University Press

the value predicted by a simple mixed circuit model.[14] Further investigation and a comparison with the Hashin–Shtrikman model[108,109] are needed.

IV. OXIDE-BASED THERMOELECTRIC MODULE

Though the *ZT* values of oxides are mostly lower than the *ZT* = 1 benchmark, oxide TE modules have been constructed and studied.[110,111] Their performance is much lower than expected due mainly to the high contact resistance at oxide/metal electrode junctions, the cracking or exfoliation due to the very different thermal expansion between oxide and metal, and the difficulty of having both p-type and n-type from the same parent compound. The high operating temperatures also make the conventional electrode materials and construction procedure less viable. It was reported that employing mixture of silver paint and 6 wt% oxide powder at the junction achieved lowest contact resistance.[112] In Funahashi's group, a TE module consisting of 108 pairs of oxide legs has been fabricated, using the p-type material $Ca_{2.7}Bi_{0.3}Co_4O_9$ and the n-type material $Ca_{0.9}Yb_{0.1}MnO_3$. At a T_{hot} = 1073 K and T_{cold} = 400 K in air, a maximum power output ~12 W is obtained, yielding a power density of the module higher than 3.0 kW/m^2. The maximum value of power density ~4.2 kW/m^2 has been achieved using p-type $Ca_{2.7}Bi_{0.3}Co_4O_9$ legs and n-type $CaMn_{0.98}Mo_{0.02}O_3$ legs. In this case, the overall TE conversion efficiency is ~3%. After cycling, brittle fracture is found in the n-type $CaMnO_3$ legs, but it does not deteriorate the power output, and this problem can be alleviated by optimizing the grain size in the pulverization process.[113]

To further increase the power output, a cascade module (segmented module) has been fabricated using 14 pairs of p-type and n-type legs. Alumina substrate is used at one side of the module, forming a so-called half skeleton module (33 × 34.5 × 6.2 mm^3). A commercial Bi_2Te_3 module with dimensions of 30 × 30 × 3.6 mm^3 is used [Fig. 6(a)]. Temperature dependence of power output, P_{max}, and the power density of P_{max} are shown in Fig. 6(b). P_{max} and density of P_{max} increase with increasing temperature. At a T_{hot} = 1273 K and T_{cold} = 300 K in air, the density of P_{max} reaches 8 kW/m^2, which is twice that of the monolithic oxide module. The temperature at the interface between the oxide and Bi_2Te_3 modules must be held 453 K or lower to prevent damages to the Bi_2Te_3 module.

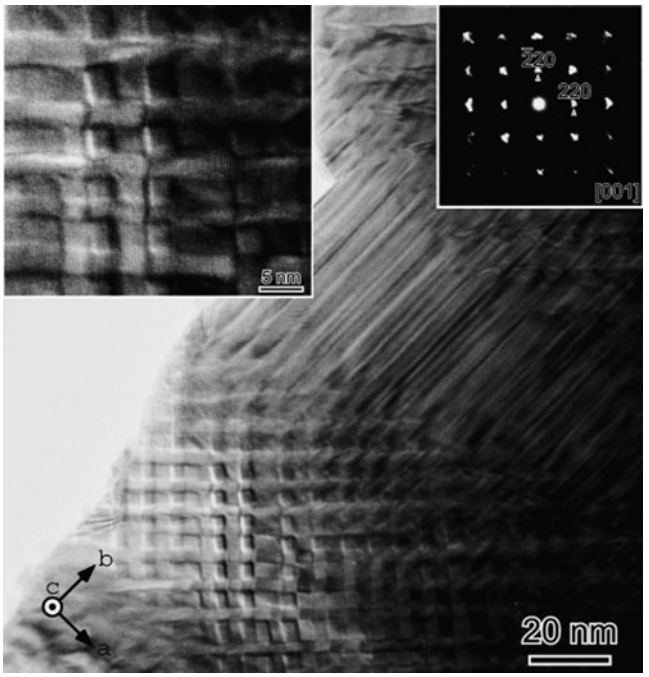


FIG. 5. Main panel: electron microscopy image of self-assembled nano-checkerboard and nanoherring structures within a $Zn(Ga,Mn)O_4$ grain. Upper-right inset: corresponding electron diffraction pattern indexed with the cubic lattice; upper-left inset: high-resolution image of the checkerboard pattern (the scale bar is 5 nm). (From Ref. 107. Copyright Japan Society of Applied Physics, reproduced with permission.)

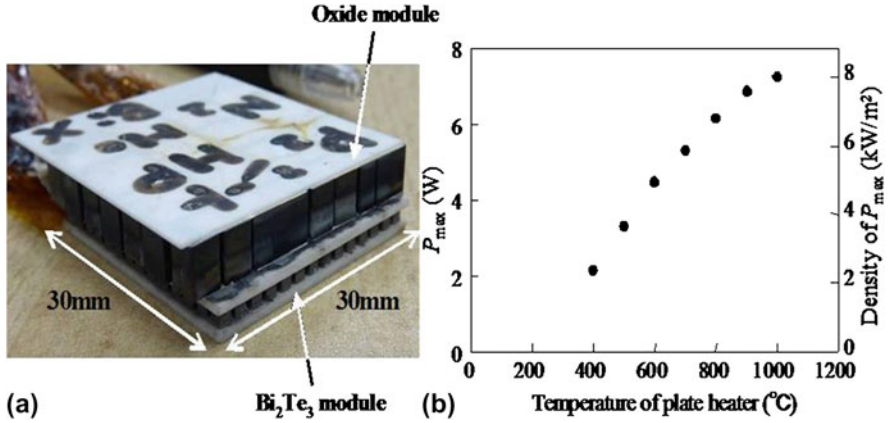


FIG. 6. (a) Pictures of oxide/Bi_2Te_3 cascade module and (b) the dependence of maximum power output on the heater temperature.

https://doi.org/10.1557/jmr.2011.108 Published online by Cambridge University Press

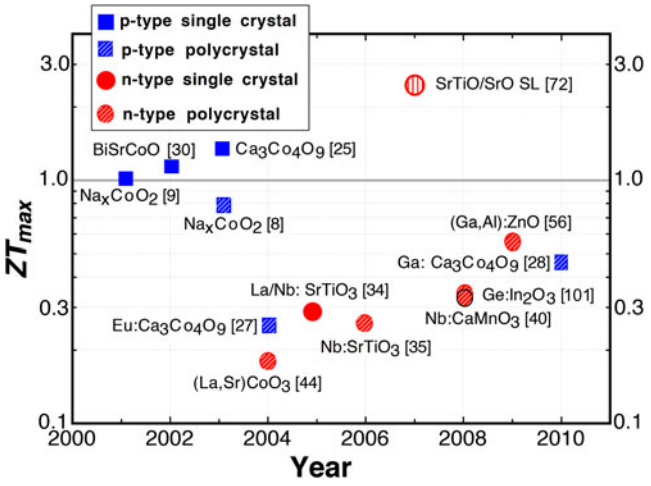


FIG. 7. The timeline of representative p-type and n-type TE oxides and their maximum figure of merit values. The number in the bracket is the reference number.

V. CONCLUDING REMARKS

The decreasing fossil fuel supplies and their environmental concerns along with the increasing energy demand worldwide impose a pressing need for improved direct thermal–electrical energy conversion via thermoelectricity. The past two decades have witnessed another rapid progress in the field of TEs since the discovery of Bi_2Te_3 and PbTe bulk materials in 1960s, and as a result, the figure of merit has been almost doubled in heavy element-based TE materials due primarily to the new paradigm of "nanostructured thermoelectrics."

On the other hand, the history of oxides TEs is fairly short. Nonetheless, the chemical and thermal stability, environmental friendliness, the low cost of raw materials, and chemical versatility are inherent merits of oxide TE materials. As shown in Fig. 7, the efforts in the layer-structured cobaltites, strontium titanate perovskites, and ZnO wurtzites have significantly improved the *ZT* of oxides in the past decade. Oxides show great potential in the application of power generation at high operation temperatures. Further enhancement of *ZT* in oxides may hinge primarily upon successful implementation of novel concepts, e.g., spin Seebeck effect,[114] energy-specific equilibrium,[115] synergistic nanostrucuring[105], technical advent of high-throughput screening of candidate materials[116], discovering new materials, e.g., $LaFeAsO_{1-y}$[117], and advances in theoretical modeling of heat and charge flows in nanocomposites.

ACKNOWLEDGMENTS

J.H. and Y.F.L thank Dr. Don Liebenberg for helpful discussion and the support from a Department of Energy/ Experimental Program to Stimulate Competitive Research (DOE/EPSCoR) Implementation Grant (No. DE-FG02-04ER-46139), and in addition, support from the SC EPSCoR Office/Clemson University cost sharing.

REFERENCES

1. T.M. Tritt, M.A. Subramanian, H. Bottner, T. Caillat, G. Chen, R. Funahashi, X. Ji, M. Kanatzidis, K. Koumoto, G.S. Nolas, J. Poon, A.M. Rao, I. Terasaki, R. Venkatasubramanian, and J. Yang: Special issue on harvesting energy through thermoelectrics: Power generation and cooling. *MRS Bull.* **31**, (2006).
2. G.S. Nolas, J. Sharp, and H.J. Goldsmid: *Thermoelectrics Basic Principles and New Materials Developments* (Springer-Verlag, Berlin Heidelberg, 2001).
3. G.A. Slack: New materials and performance limits for thermoelectric cooling, in *CRC Handbook of Thermoelectrics*, edited by D.M. Rowe (CRC Press, Boca Raton, 1995), pp. 407–440.
4. A.F. Ioffe: *Semiconductor Thermoelements and Thermoelectric Cooling* (Infosearch Ltd., London, 1957).
5. G.D. Mahan: Figure-of-merit for thermoelectrics. *J. Appl. Phys.* **65**, 1578 (1989).
6. H.J. Goldsmid: *Electronic Refrigeration* (Pion Limited, London, 1986).
7. I. Terasaki, Y. Sasago, and K. Uchinokura: Large thermoelectric power in $NaCo_2O_4$ single crystals. *Phys. Rev. B* **56**, R12685 (1997).
8. M. Ito, T. Nagira, D. Furumoto, S. Katsuyama, and H. Nagai: Synthesis of $Na_xCo_2O_4$ thermoelectric oxides by the polymerized complex method. *Scr. Mater.* **48**, 403 (2003).
9. K. Fujita, T. Mochida, and K. Nakamura: High-temperature thermoelectric properties of $Na_xCoO_{2-\delta}$ single crystals. *Jpn. J. Appl. Phys.* **40**, 4644 (2001).
10. Y. Ando, N. Miyamoto, K. Segawa, T. Kawata, and I. Terasaki: Specific-heat evidence for strong electron correlation in the thermoelectric materials $(Na,Ca)Co_2O_4$. *Phys. Rev. B* **60**, 10580 (1999).
11. Y. Wang, N.S. Rogado, R.J. Cava, and N.P. Ong: Spin entropy as the likely source of enhanced thermopower in $Na_xCo_2O_4$. *Nature* **423**, 425 (2003).
12. W. Koshibae, K. Tsutsui, and S. Maekawa: Thermopower in cobalt oxides. *Phys. Rev. B* **62**, 6869 (2000).
13. D.J. Singh and D. Kasinathan: Thermoelectric properties of Na_xCoO_2 and prospects for other oxide thermoelectrics. *J. Electron. Mater.* **36**, 736 (2007).
14. K. Koumoto, Y.F. Wang, R. Zhang, A. Kosuga, and R. Funahashi: Oxide thermoelectric materials: A nanostructuring approach. *Annu. Rev. Mater. Res.* **40**, 363 (2010).
15. M. Ohtaki: Oxide thermoelectric materials for heat-to-electricity direct energy conversion. Newslett. Kyushu Univ. G-COE program *Novel Carbon Resources Sciences*, **3**, 8 (2010). http://ncrs.cm.kyushu-u.ac.jp/ncrs2/379.html.
16. H. Ohta, K. Sugiura, and K. Koumoto: Recent progress in oxide thermoelectric materials p-type $Ca_3Co_4O_9$ and n-type $SrTiO_3$. *Inorg. Chem.* **47**, 8429 (2008).
17. C.J. Vineis, A. Shakouri, A. Marjumdar, and M.G. Kanatzidis: Nanostructured thermoelectrics: Big efficiency gains from small features. *Adv. Mater.* **22**, 3970 (2010).
18. M.G. Kanatzidis: Nanostructured thermoelectric: The new paradigm? *Chem. Mater.* **22**, 648 (2010).
19. A.J. Minnich, M.S. Dresselhaus, Z.F. Ren, and G. Chen: Bulk nanostructured thermoelectric materials: Current research and future prospects. *Energy Environ. Sci.* **2**, 466 (2009).
20. G. Mahan: Benedicks effect: Nonlocal electron transport in metals. *Phys. Rev. B* **43**, 3945 (1991).
21. L.I. Anatychuk and L.P. Bulat: Thermoelectric phenomena under large temperature gradients, in *CRC Handbook of Thermoelectrics*, edited by D.M. Rowe (CRC Press, Boca Raton, 2005), pp. 3–8.
22. P. Vaqueiro and A.V. Powell: Recent developments in nanostructured materials for high-performance thermoelectrics. *J. Mater. Chem.* **20**, 9577 (2010).

https://doi.org/10.1557/jmr.2011.108 Published online by Cambridge University Press

23. S. Li, R. Funahashi, I. Matsubara, K. Ueno, and H. Yamada: High temperature thermoelectric properties of oxide $Ca_9Co_{12}O_{28}$. *J. Mater. Chem.* **9**, 1659 (1999).
24. R. Funahashi, I. Matsubara, H. Ikuta, T. Takeuchi, U. Mizutani, and S. Sodeoka: Oxide single crystal with high thermoelectric performance in air. *Jpn. J. Appl. Phys.* **39**, L1127 (2000).
25. M. Shikano and R. Funahashi: Electrical and thermal properties of single-crystalline $(Ca_2CoO_3)_{0.7}CoO_2$ with a $Ca_3Co_4O_9$ structure. *Appl. Phys. Lett.* **82**, 1851 (2003).
26. Y. Zhou, I. Matsubara, S. Horii, T. Takeuchi, R. Funahashi, M. Shikano, J. Shimoyama, K. Kishio, W. Shin, N. Izu, and N. Murayama: Thermoelectric properties of highly grain-aligned and densified Co-based oxide ceramic. *J. Appl. Phys.* **93**, 2653 (2003).
27. D. Wang, L. Cheng, Q. Yao, and J. Li: High-temperature thermoelectrics properties of $Ca_3Co_4O_{9+\delta}$ with Eu substitution. *Solid State Commun.* **129**, 615 (2004).
28. N.V. Nong, C.-J. Liu, and M. Ohtaki: Improvement on the high temperature thermoelectric performance of Ga-doped misfit-layered $Ca_3Co_{4-x}Ga_xO_{9+\delta}$. *J. Alloy. Comp.* **491**, 53 (2010).
29. R. Funahashi, I. Matsubara, and S. Sodeoka: Thermoelectric properties of $Bi_2Sr_2Co_2O_x$ polycrystalline materials. *Appl. Phys. Lett.* **76**, 2385 (2000).
30. R. Funahashi and M. Shikano: $Bi_2Sr_2Co_2O_y$ whiskers with high thermoelectric figure of merit. *Appl. Phys. Lett.* **81**, 1459 (2002).
31. R. Funahashi and I. Matsubara: Thermoelectric properties of Pb- and Ca-doped $(Bi_2Sr_2O_4)_xCo_2$ whiskers. *Appl. Phys. Lett.* **79**, 362 (2007).
32. J.J. Shen, X.X. Liu, T.J. Zhu, and X.B. Zhao: Improved thermoelectric properties of La-doped $Bi_2Sr_2Co_2O_9$ layered misfit oxides. *J. Electron. Mater.* **44**, 1889 (2009).
33. K. Koumoto, I. Terasaki, and R. Funahashi: Complex oxide materials for potential thermoelectric applications. *MRS Bull.* **31**, 206 (2006).
34. S. Ohta, T. Nomura, H. Ohta, and K. Koumoto: High-temperature carrier transport and thermoelectric properties of heavily La- or Nb-doped $SrTiO_3$ single crystals. *J. Appl. Phys.* **97**, 034106 (2005).
35. S. Ohta, H. Ohta, and K. Koumoto: Grain size dependence of thermoelectric performance of Nb-doped $SrTiO_3$ polycrystal. *J. Ceram. Soc. Jpn.* **114**, 105 (2006).
36. Y. Cui, J. He, G. Amow, and H. Kleinke: Thermoelectric properties of n-type double substituted $SrTiO_3$ bulk materials. *Dalton Trans.* **39**, 1031 (2010).
37. T. Okuda, K. Nakanishi, S. Miyasaka, and Y. Tokura: Large thermoelectric response of metallic perovskites: $Sr_{1-x}La_xTiO_3$ ($0<\sim x<\sim 0.1$). *Phys. Rev. B* **63**, 113104 (2001).
38. A. Kosuga, Y. Isse, Y. Wang, K. Koumoto, and R. Funahashi: High-temperature thermoelectric properties of $Ca_{0.9-x}Sr_xYb_{0.1}MnO_{3-\delta}$ ($0 \le x \le 0.2$). *J. Appl. Phys.* **105**, 093717 (2009).
39. Y. Wang, Y. Sui, and W. Su: High temperature thermoelectric characteristics of $Ca_{0.9}R_{0.1}MnO_3$ (R=La, Pr, ... Yb). *J. Appl. Phys.* **104**, 093703 (2008).
40. L. Bocher, M.H. Aguirre, D. Logvinovich, A. Shkabko, and R. Robert: $CaMn_{1-x}Nb_xO_3$ ($x \le 0.08$) perovskite-type phases as promising new high-temperature n-type thermoelectric materials. *Inorg. Chem.* **47**, 8077 (2008).
41. X.Y. Huang, Y. Miyazaki, and T. Kajitani: High temperature thermoelectric properties of $Ca_{1-x}Bi_xMn_{1-y}V_yO_3$-$\delta$($0 \le x = y \le 0.08$). *Solid State Commun.* **145**, 132 (2008).
42. K. Sakai, M. Karppinen, J.M. Chen, R.S. Liu, S. Sugihara, and H. Yamauchi: Pb-for-Bi substitution for enhancing thermoelectric characteristics of $[(Bi, Pb)_2Ba_2O_{4\pm\omega}]_{0.5}CoO_2$. *Appl. Phys. Lett.* **88**, 232102 (2006).
43. W. Kobayashi, S. Hébert, D. Pelloquin, O. Pérez, and A. Maignan: Enhanced thermoelectric properties in a layered rhodium oxide with a trigonal symmetry. *Phys. Rev. B* **76**, 245102 (2007).
44. J. Androulakis, P. Migiakis, and J. Giapintzakis: $La_{0.95}Sr_{0.05}CoO_3$: An efficient room-temperature thermoelectric oxide. *Appl. Phys. Lett.* **84**, 1099 (2004).
45. W.J. Weber, C.W. Griffin, and J.L. Bates: Effects of cation substitution on electrical and thermal transport properties of $YCrO_3$ and $LaCrO_3$. *J. Am. Ceram. Soc.* **70**, 265 (1987).
46. H. Kuriyama, M. Nohara, T. Sasagawa, K. Takubo, T. Mizokawa, K. Kimura, and H. Takagi: High-temperature thermoelectric properties of delafossite oxide $CuRh_{1-x}Mg_xO_2$, *Proceedings of the 25th International Conference on Thermoelectrics*, Vienna, Austria, 97, (2007).
47. E. Guilmeau, D. Bérardan, Ch. Simon, A. Gaignan, B. Raveau, D. Ovono Ovono, and F. Delorme: Tuning the transport and thermoelectric properties of In_2O_3 bulk ceramics through doping at In-site. *J. Appl. Phys.* **106**, 053715 (2009).
48. Y.F. Wang, K.H. Lee, H. Ohta, and K. Koumoto: Thermoelectric properties of electron doped $SrO(SrTiO_3)_n$ (n=1, 2) ceramics. *J. Appl. Phys.* **105**, 103701 (2009).
49. Y.F. Wang, K.H. Lee, H. Ohta, and K. Koumoto: Fabrication and thermoelectric properties of heavily rare-earth metal-doped SrO $(SrTiO_3)_n$ (n= 1,2) ceramics. *Ceram. Int.* **34**, 849 (2008).
50. K.H. Lee, Y.F. Wang, H. Hyuga, H. Kita, H. Ohta, and K. Koumoto: Enhancement of thermoelectric performance in rare earth-doped $Sr_3Ti_2O_7$ by symmetry restoration of TiO_6 octahedra. *J. Electroceram.* **24**, 76 (2010).
51. W. Shin and N. Murayama: High performance p-type thermoelectric oxide based on NiO. *Mater. Lett.* **45**, 302 (2000).
52. R. Ishikawa, Y. Ono, Y. Miyazaki, and T. Kajitani: Low-temperature synthesis and electric properties of new layered cobaltite, Sr_xCoO_2. *Jpn. J. Appl. Phys.* **41**(Part 2), L337 (2002).
53. M. Ohtaki, T. Tsubota, K. Eguchi, and H. Arai: High-temperature thermoelectric properties of $(Zn_{1-x}Al_x)O$. *J. Appl. Phys.* **79**, 1816 (1996).
54. T. Tsubota, M. Ohtaki, K. Eguchi, and H. Arai: Thermoelectric properties of Al-doped ZnO as a promising oxide material for high-temperature thermoelectric conversion. *J. Mater. Chem.* **7**, 85 (1997).
55. S. Katsuyama, Y. Takagi, M. Ito, K. Majima, H. Nagai, H. Sakai, K. Yoshimura, and K. Kosuge: Thermoelectric properties of $(Zn_{1-y}Mg_y)_{1-x}Al_xO$ ceramics prepared by the polymerized complex method. *J. Appl. Phys.* **92**, 1391 (2002).
56. M. Ohtaki, K. Araki, and K. Yamamoto: High thermoelectric performance of dually doped ZnO ceramics. *J. Electron. Mater.* **38**, 1234 (2009).
57. H. Ohta, W.S. Seo, and K. Koumoto: Thermoelectric properties of homologous compounds in the ZnO-In_2O_3 system. *J. Am. Ceram. Soc.* **79**, 2193 (1996).
58. R. Koc and H.U. Anderson: Electrical conductivity and Seebeck coefficient of (La, Ca)(Cr, Co)O_3. *J. Mater. Sci.* **27**, 5477 (1992).
59. C. Wood and D. Emin: Conduction mechanism in boron carbide. *Phys. Rev. B* **29**, 4582 (1984).
60. H. Ohta, A. Mizutani, K. Sugiura, M. Hirano, H. Hosono, and K. Koumoto: Surface modification of glass substrate for oxide heteroepitaxy: Pastable three-dimensionally oriented layered oxide thin film. *Adv. Mater.* **18**, 1649 (2006).
61. K. Sugiura, H. Ohta, K. Nomura, M. Hirano, H. Hosono, and K. Koumoto: High electrical conductivity of layered cobalt oxide $Ca_3Co_4O_9$ epitaxial films grown by topotactic ion-exchange method. *Appl. Phys. Lett.* **89**, 032111 (2006).
62. K. Sugiura, H. Ohta, K. Nomura, T. Saito, Y. Ikuhara, M. Hirano, H. Hosono, and K. Koumoto: Thermoelectric properties of the layer cobaltite $Ca_3Co_4O_9$ epitaxial filmsfabricated by topotactic ion-exchange method. *Mater. Trans.* **48**, 2104 (2007).
63. S. Ohta, T. Nomura, H. Ohta, M. Hirano, H. Hosono, and K. Koumoto: Large thermoelectric performance of heavily Nb-doped

https://doi.org/10.1557/jmr.2011.108 Published online by Cambridge University Press

$SrTiO_3$ epitaxial film at high temperature. *Appl. Phys. Lett.* **87**, 092108 (2005).
64. D. Kurita, S. Ohta, K. Sugiura, H. Ohta, and K. Koumoto: Carrier generation and transport properties of heavily Nb-doped anatase TiO_2 epitaxial films at high temperatures. *J. Appl. Phys.* **100**, 096105 (2006).
65. K.H. Lee, A. Ishizaki, S.W. Kim, H. Ohta, and K. Koumoto: Preparation and thermoelectric properties of heavily Nb-doped $SrO(SrTiO_3)_1$ epitaxial films. *J. Appl. Phys.* **102**, 033702 (2007).
66. H. Ohta, K. Nomura, M. Orita, M. Hirano, K. Ueda, T. Suzuki, Y. Ikuhara, and H. Hosono: Single-crystalline films of $InGaO_3(ZnO)$m (m=integer) homologous phase grown by reactive solid-phase epitaxy. *Adv. Funct. Mater.* **13**, 139 (2003).
67. J.P. Dismukes, L. Ekstrom, E.F. Steigmeier, I. Kudman, and D.S. Beers: Thermal and electrical properties of heavily doped Ge-Si alloys up to 1300°K. *J. Appl. Phys.* **35**, 2899 (1964).
68. S. Ishiwata, I. Terasaki, Y. Kusano, and M. Takano: Transport properties of misfit-layered cobalt oxide $[Sr_2O_{2-\delta}]_{0.53}CoO_2$. *J. Phys. Soc. Jpn.* **75**, 104716 (2006).
69. K. Kato, M. Yamamoto, S. Ohta, H. Muta, K. Kurosaki, S. Yamanaka, H. Iwasaki, H. Ohta, and K. Koumoto: The effect of Eu substitution on thermoelectric properties of $SrTi_{0.8}Nb_{0.2}O_3$. *J. Appl. Phys.* **102**, 116107 (2007).
70. H. Muta, A. Ieda, K. Kurosaki, and S. Yamanaka: Substitution effect on the thermoelectric properties of alkaline earth titanate. *Mater. Lett.* **58**, 3868 (2004).
71. M. Yamamoto, H. Ohta, and K. Koumoto: Thermoelectric phase diagram in a $CaTiO_3$–$SrTiO_3$–$BaTiO_3$ system. *Appl. Phys. Lett.* **90**, 072101 (2007).
72. H. Ohta, S.W. Kim, Y. Mune, T. Mizoguchi, K. Nomura, S. Ohta, T. Nomura, Y. Nakanishi, Y. Ikuhara, M. Hirano, H. Hosono, and K. Koumoto: Giant thermoelectric Seebeck coefficient of a two-dimensional electron gas in $SrTiO_3$. *Nat. Mater.* **6**, 129 (2007).
73. Y. Mune, H. Ohta, K. Koumoto, T. Mizoguchi, and Y. Ikuhara: Enhanced Seebeck coefficient of quantum-confined electrons in $SrTiO_3/SrTi_{0.8}Nb_{0.2}O_3$ superlattices. *Appl. Phys. Lett.* **91**, 192105 (2007).
74. K. H. Lee, Y. Mune, H. Ohta, and K. Koumoto: Thermal stability of giant thermoelectric Seebeck coefficient for $SrTiO_3/SrTi_{0.8}Nb_{0.2}O_3$ superlattices at 900 K. *Appl. Phys. Express*. **1**, 015007 (2008).
75. N. Daude, C. Gout, and C. Jouanin: Electronic band structure of titanium dioxide. *Phys. Rev. B* **15**, 3229 (1977).
76. H. Ohta, R. Huang, and Y. Ikuhara: Large enhancement of the thermoelectrics Seebeck coefficient for amorphous oxide semiconductor superlattices with extremely thin conductive layers. *Phys. Status Solidi RRL* **2**, 105 (2008).
77. L.D. Hicks and M.S. Dresselhaus: Effect of quantum-well structures on the thermoelectric figure of merit. *Phys. Rev. B* **47**, 12727 (1993).
78. By low dimensional, we mean that the system size in one or more directions is comparable with the wavelength or the mean free path of a quantum particle or an excitation.
79. L.D. Hicks, T.C. Harman, X. Sun, and M.S. Dresselhaus: Experimental study of the effect of quantum-well structures on the thermoelectric figure of merit. *Phys. Rev. B* **53**, 10493 (1996).
80. J.P. Heremans: Low-dimensional thermoelectricity. *Acta Physiol. Pol.* **108**, 609 (2005).
81. P. Pichanusakorn and P. Bandaru: Nanostructured thermoelectrics. *Mater. Sci. Eng., R* **67**, 19 (2010).
82. We hereafter use the generic term "nanostructured material" to represent the low-dimensional systems and the nanocomposites in view of that classical and quantum-size effects in these systems are basically the same.
83. A.I. Hochbaum, R. Chen, R.D. Delgado, W. Liang, E.C. Garnett, M. Najarian, A. Marjumdar, and P. Yang: Enhanced thermoelectric performance of rough silicon nanowires. *Nature* **451**, 163 (2008).
84. A.I. Bouake, Y. Bunimovich, J. Tahir-Kheli, J.K. Yu, W.A. Goddard, III, and J.R. Heath: Silicon nanowires as efficient thermoelectric materials. *Nature* **451**, 168 (2008).
85. R. Yang and G. Chen: Thermal conductivity modeling of periodic two-dimensional nanocomposites. *Phys. Rev. B* **69**, 195316 (2004).
86. M.S. Dresselhaus, G. Chen, M.Y. Tang, R. Yang, H. Lee, D. Wang, Z. Ren, J.-P. Fleurial, and P. Gogna: New direction for low-dimensional thermoelectric materials. *Adv. Mater.* **19**, 1043 (2007).
87. D.L. Medlin and G.J. Snyder: Interfaces in bulk thermoelectric materials: A review for current opinion in colloid and interface science. *Curr. Opin. Colloid Interface Sci.* **14**, 226 (2009).
88. D.J. Bergman and O. Levy: Thermoelectric properties of a composite medium. *J. Appl. Phys.* **70**, 6821 (1991).
89. J.M.O. Zide, D. Vashaee, Z.X. Bian, G.H. Zeng, J.E. Bowers, and A. Shakouri: Demonstration of electron filtering to increase the Seebeck coefficient in $In_{0.53}Ga_{0.47}As/In_{0.53}Ga_{0.28}Al_{0.19}As$ superlattices. *Phys. Rev. B* **74**, 205335 (2006).
90. M. Zebarjadi, K. Esfarjani, S. Shakouri, Z.X. Bian, J.H. Bahk, and G.H. Zeng: Effect of nanoparticles on electron and thermoelectric transport. *J. Electron. Mater.* **38**, 954 (2009).
91. D. Li, Y. Wu, and R. Fan, P. Yang, and A. Marjumdar: Thermal conductivity of Si/SiGe superlattice nanowires. *Appl. Phys. Lett.* **83**, 3186 (2003).
92. W. Kim, J. Zide, A. Gossard, D. Klenov, S. Stemmer, A. Shakouri, and A. Marjumdar: Thermal conductivity reduction and thermoelectric figure of merit increase by embedding nanoparticles in crystalline semiconductors. *Phys. Rev. Lett.* **96**, 045901 (2006).
93. G. Joshi, H. Lee, Y. Lan, X. Wang, G. Zhu, D. Wang, R.W. Gould, D.C. Cuff, M.Y. Tang, M.S. Dresselhaus, G. Chen, and Z. Ren: Enhanced thermoelectric figure-of-merit in nanostructured p-type silicon germanium bulk alloys. *Nano Lett.* **8**, 4670 (2008).
94. C. Chiritescu, D.G. Cahill, N. Nguyen, D. Johnson, A. Bodapati, P. Keblinski, and P. Zschack: Ultra low thermal conductivity in disordered layer WSe_2 crystals. *Science* **315**, 351 (2006).
95. G.J. Snyder and E.S. Toberer: Complex thermoelectric materials. *Nat. Mater.* **7**, 105 (2008).
96. D.G. Cahill, S.K. Watson, and R.O. Pohl: Lower limit to the thermal conductivity of disordered crystals. *Phys. Rev. B* **46**, 6131 (1992).
97. A. Watanabe, T. Fukui, K. Nogi, Y. Kizaki, Y. Noguchi, and M. Miyayama: High-quality lead-free ferroelectric ceramics prepared from flash-creating-method-derived nanopowder. *J. Ceram. Soc. Jpn.* **114**, 97 (2006).
98. X.Y. Zhao, X. Shi, L.D. Chen, W.Q. Zhang, S.Q. Bai, Y.Z. Pei, and X.Y. Li: Synthesis of $Yb_yCo_4Sb_{12}/Y_2O_3$ composites and their thermoelectric properties. *Appl. Phys. Lett.* **89**, 092121 (2006).
99. E. Alleno, L. Chen, C. Chubilleau, B. Lenoir, O. Rouleau, M.F. Trichet, and B. Villeroy: Thermal conductivity reduction in $CoSb_2$-CeO_2 nanocomposites. *J. Electron. Mater.* **39**, 1966 (2010).
100. Z. He, C. Stiewe, D. Platzek, G. Karpinski, E. Muller, S. Li, M. Torpak, and M. Muhammed: Effect of ceramic dispersion on thermoelectric properties of nano-$ZrO_2/CoSb_3$ composites. *J. Appl. Phys.* **101**, 043707 (2007).
101. D. Berardan, E. Guilmeau, A. Maignan, and B. Raveau: In_2O_3:Ge, a promising n-type thermoelectric oxide composite. *Solid State Commun.* **146**, 97 (2008).
102. N. Wang, L. Han, Y. Ba, Y. Wang, C. Wan, K. Fujinami, and K. Koumoto: Effects of YSZ additions on thermoelectric properties of Nb-doped strontium titanate. *J. Electron. Mater.* **39**, 1777 (2010).
103. N. Wang, L. Han, H. He, Y. Ba, and K. Koumoto: Effects of mesoporous silica addition on thermoelectric properties of Nb-doped $SrTiO_3$. *J. Alloy. Comp.* **497**, 308 (2010).

https://doi.org/10.1557/jmr.2011.108 Published online by Cambridge University Press

104. N. Wang, H. He, Y. Ba, C. Wan, and K. Koumoto: Thermoelectric properties of Nb-doped $SrTiO_3$ ceramics enhanced by potassium titanate nanowires addition. *J. Ceram. Soc. Jpn.* **118**, 1098 (2010).
105. J.R. Sootsman, D.Y. Chung, and M.G. Kanatzidis: New and old concepts in thermoelectric materials. *Angew. Chem. Int. Ed.* **48**, 8616 (2009).
106. S. Yeo, Y. Horibe, S. Mori, C.M. Tseng, C.H. Chen, A.G. Khachaturyan, C.L. Zhang, and S.-W. Cheong: Solid-state self-assembly of nanocheckerboards. *Appl. Phys. Lett.* **89**, 233120 (2006).
107. A. Kosuga, K. Kurosaki, K. Yubuta, A. Charoenphakdee, S. Yamanaka, and R. Funahashi: Thermal conductivity characterization in bulk Zn(Mn, Ga)O_4 with self-assembled nanocheckerboard structures. *Jpn. J. Appl. Phys.* **48**, 010201 (2009).
108. Z. Hashin and S. Shtrikman: On some variational principles in anisotropic and non-homogeneous elasticity. *J. Mech. Phys. Solids* **10**, 335 (1962).
109. Z. Hashin and S. Shtrikman: Extremum principles for elastic heterogeneous media with imperfect interfaces and their application to bounding of effective moduli. *J. Mech. Phys. Solids* **10**, 343 (1962).
110. I. Matsubara, R. Funahashi, T. Takeuchi, S. Sodeoka, T. Shimizu, and K. Ueno: Fabrication of an all-oxide thermoelectric power generator. *Appl. Phys. Lett.* **78**, 3627 (2001).
111. W. Shin, N. Murayama, K. Ikeda, and S. Sago: Thermoelectric power generation using Li-doped NiO and (Ba, Sr)PbO_3 module. *J. Power Sources* **103**, 80 (2001).
112. R. Funahashi, S. Urata, K. Mizuno, T. Kouuchi, and M. Mikami: $Ca_{2.7}Bi_{0.3}Co_4O_9$-$La_{0.9}Bi_{0.1}NiO_3$ thermoelectric devices with high output power density. *Appl. Phys. Lett.* **85**, 1036 (2004).
113. S. Urata, R. Funahashi, T. Mihara, A. Kosuga, S. Sodeoka, and T. Tanaka: Power generation of a p-Type $Ca_3Co_4O_9$/n-type $CaMnO_3$ module. *Int. J. Appl. Ceram. Technol.* **4**, 535 (2007).
114. K. Uchida, J. Xiao, H. Adachi, J. Ohe, S. Takahashi, J. Leda, T. Ota, Y. Kajiwara, U. Umezawa, H. Kawai, G.E.W. Bauer, S. Maekawa, and E. Saitoh: Spin Seebeck insulator. *Nat. Mater.* **9**, 894 (2010).
115. T.E. Humphery and K. Linke: Reversible thermoelectric nanomaterials. *Phys. Rev. Lett.* **94**, 096601 (2005).
116. R. Funanashi, M. Mikami, S. Urata, M. Kitawaki, T. Kouuchi, and K. Mizuno: High-throughput screening of thermoelectric oxides and power generation modules consisting of oxide unicouples. *Meas. Sci. Technol.* **16**, 70 (2005).
117. K. Kihou, C.H. Lee, K. Miyazawa, P.M. Shirage, A. Iyo, and H. Eisaki: Thermoelectric properties of $LaFeAsO_{1-y}$ at low temperature. *J. Appl. Phys.* **108**, 033703 (2010).

https://doi.org/10.1557/jmr.2011.108 Published online by Cambridge University Press